Hydrostatic Pressure Regulates Microbial Structuring And Metabolic Functions In The Pelagic Ocean

Ying Liu
Shanghai Ocean University https://orcid.org/0000-0002-8978-378X
Mengchu Zeng
China University of Geosciences
Zhe Xie
Shanghai Ocean University
Daliang Ning
University of Oklahoma: The University of Oklahoma
Jizhong Zhou
University of Oklahoma: The University of Oklahoma
Xi Yu
Shanghai Ocean University
Rulong Liu
Shanghai Ocean University
Li Zhang
China University of Geosciences
Jiasong Fang (jsfang@shou.edu.cn)
Shanghai Ocean University https://orcid.org/0000-0001-8963-5480

Research

Keywords: hydrostatic pressure, particle-attached microorganisms, free-living microorganisms, particulate organic carbon, diatom detritus, DNA-SIP, metatranscriptomics

Posted Date: June 22nd, 2021

DOI: https://doi.org/10.21203/rs.3.rs-614724/v1

Abstract

Background: Microbial-mediated decomposition of particulate organic matter (POM) during its downward transport from the surface to the deep ocean constitutes a critical component of the global ocean carbon cycle. However, the extent to which hydrostatic pressure affects microbial community structuring and metabolic functions is largely underexplored.

Results: In this study, we investigated microbial community succession, phylogenetic and functional diversity, and metabolic capabilities during POM decomposition by particle-attached (PAM) and free-living microorganisms (FLM) under increasing hydrostatic pressures. Diatom-originated ^{13}C-labeled POM was used to incubate surface water microbial communities from the East China Sea (ECS) at pressures of 0.1, 20, and 40 MPa (megapascal). Our results showed that the PAM and FLM communities exhibited contrasting patterns and pressure-dependencies in diversity, richness, and evenness. Microbial assembly was governed predominantly by stochastic processes at low pressure and by deterministic processes at high pressure. Network analysis uncovered the non-randomly structured PAM and FLM communities and clusters of operational taxonomic units (OTUs) that reflected different functional and ecological capacities of the subgroups. Metatranscriptomic analysis revealed that gene expression of known metabolic pathways (carbohydrate, amino acid, and energy production) varied greatly with pressure and between PAM and FLM. Furthermore, the FLM communities maintained higher metabolic activities than the PAM communities at high pressures, indicating the apparent difference in resource utilization capacity and ecological functions of PAM and FLM in different pelagic zones of the ocean. Overall, we demonstrated that marine heterotrophic microbial assemblage patterns were non-random; the PAM were crucial in community structuring, whereas the FLM played more important roles in POM decomposition in the deep.

Conclusions: Our results provide detailed insights into and increased mechanistic understanding of the structuring and succession of microbial communities and metabolic functions associated with POM degradation in the pelagic ocean.

Background

Marine microbial physiology and trophic styles have often been linked to life strategies, including microbial motility, gene expression and substrate acquisition, and ecological functions in the ocean. This linkage is increasingly recognized and documented for the ecological dichotomy of heterotrophic prokaryotes in the marine environment, the particle-attached (PA), and free-living (FL) microbes (PAM, FLM). PAM and FLM play important but different roles in the global ocean carbon cycle, particularly in the decomposition of particulate organic carbon (POC) and degradation of dissolved organic carbon (DOC) [1–4]. It has been shown that PAM and FLM had different morphological, physiological, and genomic characteristics. For instance, PAM cells are often found larger in size and have higher enzymatic and metabolic activities than their FLM counterparts in the surrounding water [5–7]. Additionally, some studies showed that the abundance and diversity of marine PAM were often less than those of FLM

counterparts [6, 8, 9]. Other studies revealed that the PAM and FLM communities often differ phylogenetically in various marine environments [10–13].

However, these previous studies have been limited to alpha- and/or beta-diversity analysis of shallow water microorganisms, and do not determine the associations between PAM and FLM, and how changes in environmental conditions (e.g., temperature, pressure, and composition of organic matter in the water column) affect microbial lifestyles and metabolisms. In this regard, change in hydrostatic pressure is particularly important, as microbes attached to the descending particles would experience the direct effect of significantly changed pressure from surface water to the deep ocean [4]. Hydrostatic pressure affects bacterial physiology, metabolic activity, and carbon cycling in the deep ocean [14–16]. Previous studies showed that increasing pressure resulted in reduced bacterial cell numbers [17] and bacterial metabolic activity [18]. A recent DNA-stable isotope probing (SIP)-based study showed that only a subset of the microbes, particularly the rare bacterial taxa, were actively involved in POM decomposition and degradation [19].

In this study, we examined microbial interactions, community assembly, and shifting in metabolic capacities of PAM and FLM in POM (i.e., diatom detritus) decomposition and resource utilization under different hydrostatic pressures by combining the sensitive DNA-SIP technique and the informative metatranscriptomic sequencing. We hypothesize that the PAM and FLM communities are assembled via different community assembly processes, and hydrostatic pressure exerts significant effects on microbial metabolic capabilities. We further predict that PAM and FLM communities play a different metabolic role in POM decomposition, and their relative contributions varied at different hydrostatic pressures. This study aimed to test this hypothesis and determine how different microbes respond to pressure changes in community dynamics and metabolic functions.

Results

Microbial diversity, richness, and evenness

A total of 1,033 OTUs were identified from 3,615,779 high-quality sequences from the ECS in-situ surface water (ISW), with 929 and 835 OTUs (731 shared OTUs) for communities of PAM and FLM, respectively. The Good's coverage ranged from 99.8 to 100%, suggesting that the diversities of the microbial communities were well covered in this study.

Overall, the PAM and FLM communities showed contrasting patterns and pressure dependencies in diversity, richness, and evenness. Microbial diversity and richness showed a decreasing trend with growth pressure, whereas evenness exhibited a more varied pattern. In general, the FLM communities had higher alpha-diversity than the PAM communities at low pressure (0.1 MPa), and comparable values at high pressures (20 and 40 MPa) (Fig. 1). On the other hand, the PAM assemblages had higher evenness than the FLM communities at all pressures. However, the two groups had nearly the same species richness at all three pressures.

In this study, we define active communities as those with relative OTU abundance ≥ 1%, i.e., the abundance of an OTU retrieved in the ^{13}C-heavy DNA fraction minus the corresponding abundance in the ^{12}C-heavy DNA fraction after incubations (Additional file 1: Figure S1) [19, 20]. The active PAM and FLM assemblages exhibited more contrasting differences in the three indices. For instance, compared to PAM, the FLM communities had higher alpha diversity, and the difference became even larger at high pressures. PAM showed much higher evenness than the FLM communities, especially at 20 MPa (Fig. 1). Overall, microbial diversity and species richness decreased precipitously with growth pressure, whereas evenness exhibited an increasing trend.

Microbial community structure

In the in-situ seawater samples, the dominant groups were *Gammaproteobacteria* (35% of the total reads) and *Bacteroidetes* (33%) in PAM, and *Alphaproteobacteria* (27%) and Actinobacteria (24%) in FLM (Additional file 1: Figure S2). After incubation, the dominated groups in PAM communities shifted to *Gammaproteobacteria* (44%) and *Gracilibacteria* (25%) at 0.1 MPa, *Gammaproteobacteria* (81%) and *Bacteroidetes* (11%) at 20 MPa, and *Bacteroidetes* (48%) and *Gammaproteobacteria* (38%) at 40 MPa (Additional file 1: Figure S2). Meanwhile, the FLM communities were dominated by *Gammaproteobacteria* (39%) and *Gracilibacteria* (22%), by *Gammaproteobacteria* (78%) and *Alphaproteobacteria* (17%), and by *Gammaproteobacteria* (45%) and *Bacteroidetes* (29%) at 0.1, 20, and 40 MPa, respectively (Additional file 1: Figure S2).

The dominant active taxa in the PAM assemblages were *Alphaproteobacteria* (9%) at 0.1 MPa, *Gammaproteobacteria* (20%) at 20 MPa, and *Bacteroidetes* (23%) at 40 MPa. Similarly, the predominant active FLM communities were *Gammaproteobacteria* (8%), *Gammaproteobacteria* (14%), and *Bacteroidetes* (17%) at 0.1, 20, and 40 MPa, respectively (Additional file 1: Figure S3a). At genus level, the active PAM microbial taxa were mainly affiliated with *Alteromonas* (7%) and *Tenacibaculum* (4%); *Pseudoalteromonas* (23%) and *Alteromonas* (4%); and *Tenacibaculum* (26%) and *Alteromonas* (8%) at 0.1, 20, and 40 MPa, respectively (Fig. 2a and Additional file 1: Table S1). The active FLM genera included *Vibrio* (5%) and *Marinomonas* (5%); *Pseudoalteromonas* (8%) and *Amphritea* (6%); *Tenacibaculum* (17%) and *Lentibacter* (3%) at 0.1, 20, and 40 MPa, respectively (Fig. 2a and Additional file 1: Table S1).

Venn diagrams showed that the PAM and FLM assemblages shared a high proportion of OTUs at the three pressures, from 63 to 73% for the entire communities (Additional file 1: Figure S4). Interestingly, the proportions of shared OTUs between the active PAM and FLM assemblages were much lower (14 to 27%) than observed in the total communities (Additional file 1: Figure S4). It is also instructive to observe that three distinct clusters were identified by NMDS analysis that corresponded to the microbial communities at 0.1, 20, and 40 MPa, irrespective of microbial lifestyles, in both the total and active communities (Fig. 3). This result suggests that the microbial communities were significantly influenced by hydrostatic pressure ($P < 0.05$) (Fig. 3). However, slight differences were observed between the PAM and FLM communities at all three pressures ($P > 0.05$; Fig. 3).

Microbial community assembly

To determine the relative importance of stochastic vs. deterministic ecological processes in microbial community assembly, we calculated the taxonomic normalized stochasticity ratio (NST) [21] for PAM and FLM communities (Table 1 and Fig. 4). In microbial community assembly, deterministic processes mainly include biotic (competition and other biotic interactions) and abiotic factors (environmental filtering) that lead to species sorting; stochastic processes include neutral dispersal (immigration and emigration), drift (random birth and death events), and diversification [22].

Table 1
Variations of the normalized stochasticity ratio (*NST*) for the PAM and FLM microbial communities at 0.1, 20, and 40 MPa, respectively, after the addition of diatom detritus. The microbial composition tended to more stochastic (*NST* > 50%) or more deterministic (*NST* < 50%) based on the calculation of *NST*.

Groups	PAM		FLM	
	NST values	STDEV	*NST* values	STDEV
0.1 MPa	85%	8%	73%	9%
20 MPa	40%	6%	40%	8%
40 MPa	63%	7%	50%	8%

Our results showed that stochastic processes governed the PAM (NST = 85%) and FLM communities (73%) after incubated with diatom detritus at 0.1 MPa. However, deterministic processes predominated the PAM and FLM communities at 20 MPa, with the NST values of 40% and 40%, respectively. The PAM and FLM communities tended to more stochastic at 40 MPa, with the NST values of 63% and 50%, respectively (Table 1 and Fig. 4).

Ecological networks of PAM and FLM and their topological features

We sought to determine microbial associations based on network analysis. Six networks were constructed for the PAM and FLM communities. The constructed networks consisted of 274 OTUs, with nodes representing OTUs and links representing correlations (positive or negative) between OTUs (Fig. 5). The overall topology indexes suggest that the networks were scale-free (R^2 = 0.43–0.81; Additional file 1: Table S2), implying that a few hub OTUs (taxa) in the networks were highly connected while most OTUs had a few connections [23, 24]. All networks exhibited small-world features, as indicated by the higher average path distance (GD) and average clustering coefficient (avgCC) compared to the respective randomized networks (Additional file 1: Table S2), i.e., microbes were highly and efficiently connected in the small-world networks. Overall, nodes in both the PAM and FLM networks tended to be more negatively correlated, as indicated by the number of total positive/negative links, 570/620 and 279/602 for PAM and FLM networks, respectively. However, the number of positive links increased with hydrostatic pressure for both the PAM and FLM networks, and the negative links decreased with pressure for the FLM networks, and first decreased and then increased for the PAM networks (Additional file 1: Table S2).

The sizes of the networks differed greatly between the PAM and FLM networks. For PAM networks, 29 modules were generated, and the number of modules decreased with pressure (Fig. 5 and Additional file 1: Table S2). The node number also significantly reduced with pressure, from 146 at 0.1 MPa to 105 and 99 at 20 and 40 MPa, respectively; in contrast, the number of links increased with pressure, from 347 to 391 and 452. Meanwhile, the connectivity indexes, including avgK (average connectivity), avgCC (indicating the degree to which the nodes tend to cluster together), and density (indicating network complexity), increased with pressure, suggesting that increasing hydrostatic pressure enhanced network complexity and microbial interactions for the PAM communities. However, GD, modularity, centralization of betweenness (CB), centralization of stress centrality (CS), and module number decreased with pressure (Fig. 5 and Additional file 1: Table S2). The nodes in the PAM networks were affiliated with 21 phyla, mainly Proteobacteria (44.1–66.6%), Bacteriodetes (2.3–17.3%), and Firmicutes (5.5–14.3%), with proteobacteria being most abundant in the PAM networks (Additional file 1: Figure S5). Overall, the PAM networks were consisted of highly connected OTUs forming structured modules.

The FLM networks were slightly larger (32 modules). Nodes in the FLM networks were mainly associated with Proteobacteria (21.8–60.2%), Bacteriodetes (1.1–5.4%), and Verrucomicrobia (0.6–4.9%) (Additional file 1: Figure S5). The FLM network topologies exhibited different variation patterns with hydrostatic pressure. The number of nodes and modules, CS, and R^2 of power-law decreased steadily with pressure. Interestingly, the FLM networks showed a consistent variation pattern in avgK, avgCC, modularity, and the total number of links, i.e., decrease from 0.1 to 20 MPa, followed by increase (with the value higher than those at 0.1 and 20 MPa) at 40 MPa (Fig. 5 and Additional file 1: Table S2).

Module hubs and connectors are considered keystone species and play an essential role in structuring ecological networks [23, 25, 26]. In our study, module hubs and connectors were identified based on the within- (Zi) and among-module (Pi) connection degrees of individual node. A total of 9 module hubs and 46 connectors were identified in the constructed networks (Additional file 1: Table S2). However, no network hubs were found for any of the constructed networks. Examining the topological properties shows that all three PAM networks had one or more module hubs ($Zi \geq 2.5$, $Pi < 0.62$), whereas only one module hub (OTU930) was found in the FLM networks (0.1 MPa FLM). Furthermore, some of the identified module hubs were members of unclassified genera (Additional file 1: Table S2). For example, members from *Alteromonas* (OTU118, 0.02%), *Marinomonas* (OTU988, 2.16%), *Pseudogulbenkiania* (OTU862, 0.01%), and unclassified Parachlamydiaceae (OTU 492, 0.01%) in the PAM communities made up all the module hubs at 0.1 MPa. Interestingly, the norank Cyanobacteria (OTU590, 0.011%) was the only module hub at 20 MPa PAM, while module hubs at 40 MPa PAM were from *Tropicimonas* (OTU578, 0.006%), unclassified Parcubacteria (OTU864, 0.011%) and unclassified Alphaproteobacteria Incertae Sedis (OTU979, 0.01%) (Additional file 1: Table S2).

Connectors were detected in all PAM and FLM networks, but the distribution and taxa compositions were rather different between the PAM and FLM networks. At pressures of 0.1 and 20 MPa, there were much more connectors in the FLM networks than in the PAM networks, and it is opposite at high pressure (40 MPa). Furthermore, the number of connectors identified in the FLM networks (35) was much more than

that in the PAM networks (11). Thus, there were more module hubs in the PAM networks and more connectors in the FLM networks, suggesting the different ecological roles of the PAM and FLM communities (Additional file 1: Table S2).

Genetic repertoires and metabolic functions of PAM and FLM

Metatranscriptome sequencing analysis of ^{13}C-labeled RNA allowed us to detect 26 most abundant active genera (> 1% in the relative abundance of mRNA transcripts) (Fig. 2b and Additional file 1: Table S3-S4). In the PAM fraction, the most active microbial taxa were *Alteromonas* (38%) and *Marinomonas* (21%) at 0.1 MPa, *Pseudoalteromonas* (31%) and *Alteromonas* (8%) at 20 MPa, and *Alteromonas* (32%) and *Tenacibaculum* (19%) at 40 MPa. In the FLM fraction, the most active taxa were *Amphritea* (46%) and *Pseudoalteromonas* (23%) at 0.1 MPa; *Amphritea* (32%) and *Pseudoalteromonas* (27%) at 20 MPa, and *Pseudoalteromonas* (25%) and *Vibrio* (25%) at 40 MPa (Fig. 2b and Additional file 1: Table S4). Thus, the active taxa identified based on metatranscriptome analysis are comparable to those detected by DNA-SIP, except for those at 0.1 and 40 MPa, where different genera for PAM at 0.1 MPa and for FLM at 0.1 and 40 MPa were observed.

The 45 most transcribed functional genes (FPKM≥1000), the annotated enzymes and related metabolic pathways are shown in Fig. 6 and Table S5 (Additional file 1). The PAM and FLM communities differed in their genetic repertoires. First, the genetic machinery for fast growth varied distinctly between the PA and FL microbes. For instance, the FLM communities exhibited steadily increased expressions with pressure in genes related to genetic information processing such as, translation, DNA replication and repair, and ribosome biogenesis (Additional file 1: Figure S6 and Table S5). The PAM fraction, on the other hand, showed a more varied pattern in expressions of the same genes. Second, expressions of genes related with intake of extracellular compounds (i.e., membrane transport, signal transduction, cell motility proteins and the two-component system) showed the similar patterns as the genetic machinery described above, that is, increased expressions at high pressure (40 MPa) for the PAM as well as FLM assemblages (Additional file 1: Figure S6 and Table S5). Finally, both PAM and FLM showed inflated fractions of genes involved in protein folding stability, sorting and degradation, suggesting the global regulation of protein folding and trafficking in environmental adaptation and resource utilization at high pressures (Additional file 1: Figure S6 and Table S5).

Furthermore, the PAM and FLM assemblages differed significantly in the common metabolic processes, carbohydrate, amino acid, lipid, nucleotide, and energy metabolism.

The carbohydrate metabolic processes involved by the active microorganisms included glycolysis/gluconeogenesis, the citrate cycle (TCA cycle), and the pentose phosphate pathway (Fig. 7). The six highly expressed enzymes involved in glycolysis/gluconeogenesis, pyruvate dehydrogenase (PDH) E1 component [EC:1.2.4.1], phosphoenolpyruvate carboxykinase (ATP) [EC:4.1.1.49], glyceraldehyde 3-phosphate dehydrogenase (GAPDH) [EC:1.2.1.12], dihydrolipoamide dehydrogenase (DLD) [EC:1.8.1.4], aldehyde dehydrogenase (NAD^+) (ALDH, EC:1.2.1.3), fructose-bisphosphate aldolase,

class II [EC:4.1.2.13], were transcribed mainly by *Alcanivorax*, *Lentibacter*, *Marinomonas*, *Pseudoalteromonas* and *Vibrio*, which were dominant members of the FLM assemblages (Fig. 2b). The four main enzymes mediating the TCA cycle, malate dehydrogenase [EC:1.1..1.37], succinate dehydrogenase flavoprotein subunit [EC:1.3.99.1], succinate dehydrogenase iron-sulfur protein [EC:1.3.99.1], and succinyl-CoA synthetase beta subunit [EC:6.2.1.5], were mostly transcribed by *Pseudoalteromonas*, a very abundant taxon presented in both the PAM and FLM assemblages (Fig. 8).

The amino acid metabolism included alanine, aspartate, glutamate, glycine, serine, threonine, cysteine, and methionine metabolism (Fig. 6 and Additional file 1: Table S5). The alanine dehydrogenase [EC:1.4.1.1], transcribed exclusively by *Vibrio*, was the highest expressed enzymes in alanine, aspartate, and glutamate metabolism (Fig. 8). The glycine dehydrogenase [EC:1.4.4.2] was the highest transcribed enzymes in glycine, serine, and threonine metabolism, by *Alcanivorax*, *Marinomonas*, *Pseudoalteromonas*, and *Vibrio* (Fig. 8 and Additional file 1: Table S6). The highly active enzymes implicated in cysteine and methionine metabolism were s-adenosylmethionine synthetase [EC:2.5.1.6] and cysteine synthase A [EC:2.5.1.47]. These enzymes were highly expressed by the same genera such as *Marinomonas*, *Pseudoalteromonas*, and *Vibrio* (Fig. 8 and Additional file 1: Table S6). Besides, the ketol-acid reductoisomerase [EC:1.1.1.86] was the highest transcribed enzymes in valine, leucine, and isoleucine biosynthesis (Additional file 1: Table S5).

Nucleotide metabolism mainly included purine and pyrimidine metabolism. The high expressed enzymes involved in purine metabolism include polyribonucleotide nucleotidyltransferase [EC:2.7.7.8], DNA-directed RNA polymerase subunit alpha, beta, and beta´ [EC:2.7.7.6], nucleoside-diphosphate kinase [EC:2.7.4.6], GMP synthase (glutamine-hydrolysing) [EC:6.3.5.2], and purine-nucleoside phosphorylase [EC:2.4.2.1] (Fig. 6 and Additional file 1: Table S5). These enzymes were highly expressed by *Alcanivorax*, *Amphritea*, *Idiomarina*, *Marinomonas*, *Pseudoalteromonas*, and *Vibrio* (Fig. 8 and Additional file 1: Table S6). On the other hand, thioredoxin reductase (NADPH) [EC:1.8.1.9] and CTP synthase [EC:6.3.4.2] were the highest transcribed enzymes in pyrimidine metabolism, by *Alcanivorax*, *Marinomonas*, and *Pseudoalteromonas* (Fig. 8 and Additional file 1: Table S6).

Many enzymes involved in oxidative phosphorylation (energy metabolism) were found, for instance, F-type H^+-transporting ATPase subunit a, b, alpha, beta, gamma, delta, and epsilon [EC:3.6.3.14], cytochrome o ubiquinol oxidase subunit II [EC:1.10.3.-], cb-type cytochrome c oxidase subunit III [EC:1.9.3.1], ubiquinol-cytochrome c reductase iron-sulfur subunit [EC:1.10.2.2], and ubiquinol-cytochrome c reductase cytochrome c1 subunit [EC:1.10.2.2] (Fig. 6 and Additional file 1: Table S5). The seven F-type H+-transporting ATPase subunit were transcribed by four bacterial taxa, *Alcanivorax*, *Marinomonas*, *Pseudoalteromonas*, and *Vibrio*, especially by the latter abundantly represented in the FLM assemblage at 40 MPa (Fig. 8 and Additional file 1: Table S6).

Finally, corresponding to the genetic repertoires described above, flagellin and aerobic respiration control protein ArcA were found to be highly expressed, mainly by *Marinomonas* and *Pseudoalteromonas* (Figs. 6 and 8). Among the cellular processes, we found two proteins, flagellar hook-associated protein 2 and

flagellar basal-body rod protein FlgB, were highly expressed in flagellar assembly, and the former was produced mainly by *Amphritea* and *Marinomonas*, found in both the PAM and FLM communities (Figs. 6 and 8).

Discussion

Microbial succession and community assembly processes under different pressures

Our study revealed that microbial succession and community assembly processes were significantly affected by hydrostatic pressure. NMDS analysis illustrated that communities of both PAM and FLM at the same growth pressure clustered together, irrespective of microbial lifestyle (Fig. 3). Metatranscriptome sequencing results confirmed that these clusters were associated with different functional capacities (metabolism, information processing, and directional cellular trafficking), suggesting that these clusters were functionally and ecologically important subgroups at respective hydrostatic pressure (Figs. 2b and 6). Indeed, these subgroups were comprised of different taxa, phylogenetically and functionally, at different pressures (Figs. 2b and 6). Correspondingly, both PAM and FLM communities showed obviously less stochastic assembly, denser between-taxa associations, and higher network complexity under high pressures (20 and 40 MPa) than at low pressure (0.1 MPa), suggesting pressure-induced selection of taxa with specific functions interacting with the biotic/abiotic environment.

More interestingly, PAM and FAM communities showed different responses to pressures. The PAM groups had consistently lower Shannon diversity than the FLM groups (Fig. 1), consistent with the notion that sinking particles in the ocean are carbon- and nutrient-rich microniches, explored and utilized predominantly by a few well adapted fast growers attached to the particles, the so-called r-strategists [4, 27, 28].

Our results further revealed that members of the PAM assemblages constituted most of the network module hubs, while members of the FLM communities served as most network connectors (Additional file 1: Table S2). These results indicate that the PAM assemblages played a more important role in structuring the networks and maintaining network stability, while the FLM taxa were mainly “communicators” in information processing and transfer in the networks. Surprisingly, most of the identified module hubs (44.4%) and connectors (50.0%) were unclassified at genus level and of low abundances, suggesting that taxa of the rare biosphere may play more important roles in structuring bacterial communities and that our knowledge is limited about the potentially important ecological roles of these taxa in the interacting communities of PAM and FLM in the ocean. This finding is similar to that observed in a freshwater lake [29].

Furthermore, the PAM networks had more positive associations than the FLM networks at all pressures, whereas the FLM networks had more negative links than the former at 0.1 and 20 MPa. Positive associations may include cross-feeding, co-aggregation in biofilms, co-colonization, niche overlap, whereas a negative relationship may result from amensalism, predation, and competition [23]. These results reflect the different lifestyles, or dichotomy, of marine microbes, that is, the PA microbes, as

copiotrophs in the ocean, prefer the particle-attachment life strategy, for rich resources of carbon and nutrients in the descending particulates in the water column [4, 5].

Microbial network topological properties indicate niche differentiation and differed microbial interactions under different pressures [30, 31]. Network modules can be considered as niches or microbial functional units [32, 33]. The steadily reduced modularity for the PAM networks (Additional file 1: Table S2) suggests decreased PA community segregation, whereas the increased modularity for the FLM networks reflects more niche separation of the FL communities into finer niches and functional units, perhaps around the particulates [4]. This increased compartmentalization would enhance the stability in networks of the FLM communities and increase population diversity [31, 34], consistent with our findings in alpha-diversity of the two groups of communities (Fig. 1). The avgK index indicates network complexity [31]. Compared to FLM networks, the PAM networks had relatively higher average degree (or connectivity) and higher modularity, suggesting greater network vulnerability for the PAM networks, particularly at high pressures. We postulate that these observed differences in network stability and microbial interactions between PAM and FLM can be attributed to microbial physiology, trophic lifestyles, and life strategies in the ocean. For one, compared to FLM, PAM are supposedly more closely associated between each other in microniches of the particulates [5, 35], and therefore, closer, and perhaps more efficient metabolic interactions [27, 36, 37]. For the other, the lower avgK, larger network sizes and higher microbial diversity of the FLM networks indicate greater network resilience or stability of the FLM communities [31].

Pressure-regulated metabolic activities of PAM and FLM

Hydrostatic pressure dramatically influenced microbial metabolic activity in POM decomposition and utilization. It is remarkable that expression of genes involved in various metabolic processes such as carbohydrate, amino acid, nucleotide, and energy metabolism were downregulated with pressure for PAM, and upregulated for FLM.

The expression abundance of enzymes in glycolysis/gluconeogenesis decreased with pressure in the PAM fraction while increased with pressure in the FLM fraction. For example, the expressed abundance of phosphoenolpyruvate carboxykinase (ATP) that catalyzes ATP to ADP, and fructose-bisphosphate aldolase, class II that catalyzes the reversible reactions for transferring D-fructose 1,6-bisphosphate to glycerone phosphate and D-glyceraldehyde 3-phosphate in glycolytic/gluconeogenesis [38] decreased with pressure in the PAM fraction. In contrast, the proportion of this enzyme for the FLM fraction increased with pressure. Similar variation patterns of enzyme expressions affected by pressure were observed in the TCA cycle (Fig. 7). Furthermore, FLM expressed higher activity of succinyl-CoA synthetase beta subunit at 40 MPa than PAM in the TCA cycle, the FPKM of the enzyme for FLM at 40 MPa was more than eightfold of that at 0.1 MPa. Meanwhile, the FPKM of this enzyme for FLM at 40 MPa were about 3 times that of PAM at the same pressure (Fig. 6 and Additional file 1: Table S5). These results suggest that FLM taxa maintained higher transcriptional and enzyme activity in carbohydrate metabolism than PAM at high hydrostatic pressures, and likely play a more important role in carbon cycling in the deep ocean [4]. This functional difference is probably related to microbial physiology and

life strategies in the ocean, as discussed above. Our results are consistent with the notion that growth rates and metabolic activities of free-living microorganisms are higher than those of particle-attached microorganisms in the deep ocean [37].

Pressure effect on enzyme activity of amino acid metabolism showed the same variation pattern. For instance, the transcriptional abundance of the alanine dehydrogenase in the FLM fraction increased dramatically from 8 at 0.1 MPa to 1,448 at 40 MPa, while the corresponding values in the PAM fraction decreased from 33 to 25. Also, the FPKM of glycine dehydrogenase and s-adenosylmethionine synthetase decreased for PAM while increased for FLM with increasing pressure. These results indicate that the FLM communities maintain a stronger ability and higher activity than the PAM communities for the utilization of amino acids at high pressures.

F-type H^+-transporting ATPase is a functional ATP synthase for ATP production, which is a key multi-subunit enzyme for living microorganisms meeting their energy requirements [39]. The seven F-type H^+-transporting ATPase subunits, a, b, alpha, beta, gamma, delta, and epsilon related to the oxidative phosphorylation (ko00190) in energy metabolism also exhibited the aforementioned variation pattern. The FPKM of these enzymes for the FLM were upregulated sharply with pressure and downregulated with pressure for the PAM assemblage (Fig. 6 and Additional file 1: Table S5). These observations supported the hypothesis that the FLM communities are more active in carbon and energy metabolic processes at high pressure than the PAM assemblages, and potentially play a more important ecological role in the deep ocean [19, 37].

In summary, there was a clear discrepancy in gene expressions for enzymatic activities between PAM and FLM. This differential expression can be attributed to microbial interactions and niche overlap in community assembly, affected by hydrostatic pressure. As shown in Fig. 5 and Additional file 1: Table S2, the modularity of the PAM community networks decreased significantly with pressure, so was the total number of modules. However, the average degree, and avgK which represents the frequency of microbial interactions in networks [31], increased substantially with pressure. As modules can be considered as niches or microbial functional units [32, 33], decreases in modules and modularity in PAM networks can be interpreted as reduced functional segregation or increased niche overlap, and therefore, enhanced microbial interactions and network complexity, in the PAM communities. The decreased niche differentiation is in accordance with the observed decrease in microbial diversity with pressure. This inference is also consistent with the variations in positive and negative links in PAM and FLM communities (Additional file 1: Table S2). The decreased negative associations with pressure for the FLM networks can be perceived as reduced competition, and therefore, increased utilization of POM.

Generalists or specialists, the evolving ecological roles of PAM and FLM with hydrostatic pressure in the pelagic ocean

It is believed that most marine microorganisms are generalists, but with dual lifestyles [40], and therefore, able to grow in either free-living or attached-on-particle mode [41, 42]. However, microbes can switch

lifestyles leading to species sorting, depending on the environmental conditions [43, 44]. Regardless, our results showed that hydrostatic pressure affected microbial life strategies and community assembly, which in turn influenced microbial metabolic activity and ecological functions. This is clearly demonstrated by the vastly varied metabolic activities of *Alcanivorax, Vibrio, and Marinomonas* with growth pressure.

The metabolic activity of particle-attached *Alcanivorax* decreased with pressure, while enzyme expression of the free-living *Alcanivorax* increased with pressure (Additional file 1: Table S6). For example, the FPKM of DNA-directed RNA polymerase subunit beta of PA *Alcanivorax* decreased with pressure, from 1,122 at 0.1 MPa to 156 FPKM at 40 MPa, whereas that of FL *Alcanivorax* increased sharply, from 399 at 0.1 MPa to 13,685 FPKM at 40 MPa. Similarly, the expression abundance of glyceraldehyde 3-phosphate dehydrogenase reduced from 267 at 0.1 MPa to 67 FPKM at 40 MPa for PA *Alcanivorax*, while the corresponding value increased sharply for FLM from 115 at 0.1 MPa to 2,112 FPKM at 40 MPa (Fig. 8). Additionally, it is well known that *Alcanivorax* can degrade different hydrocarbons [45], but are unable to decompose carbohydrates and amino acids [46]. Our data, however, revealed that *Alcanivorax* was able to express various enzymes in carbohydrate and amino acid metabolism. Thus, our results suggest that that the FLM communities likely play a more important role than the PAM communities in degrading recalcitrant organic matter in the deep ocean.

Conclusions

By combining DNA-SIP with metatranscriptome sequencing, we provided detailed insights into the community ecology and metabolic functions of particle-attached and free-living microbes in decomposition of diatom detritus with increasing hydrostatic pressure. This approach allowed us to piece together the community assembly processes, interactions between and the vital role served by, the PAM and FLM taxa. By exposing the same microbial communities to the same particulates (in composition and concentration) so as to eliminate other factors (like nutrient dynamics) in affecting microbial succession, we were able to pinpoint the impact of hydrostatic pressure on the metabolic and ecological functions of the PAM and FLM communities. We showed that high pressure led to obviously decreased stochasticity in microbial community assembly, higher volunability of the PAM communities and more resilience of the FLM communities. Likewise, the PAM communities exhibited decreased transcriptomic responses to increasing pressure in carbohydrate, amino acid and energy metabolism, while the FLM communities showed sharply upregulated gene expressions in these same metabolisms, suggesting the ecologically more important roles for the FLM communities in POM decomposition and carbon cycling the deep ocean. Our findings provide further ecological insights and increased mechanistic understanding on how hydrostatic pressure affected the metabolic specialization and ecological functions of members of the PAM and FLM communities.

Methods

Seawater sampling

Seawater samples were collected from water depth of 15 m at the Eastern China Sea (30°39′48″N, 122°29′48″E) in September 2018 (Additional file 1: Figure S7). The corresponding geochemical parameters of the water samples are listed in Additional file 1: Table S7.

Triplicate 3 L of the seawater was filtered sequentially through 3.0 and 0.22 μm pore-size polycarbonate membrane (47 mm; Merck Millipore Ltd.) to obtain PAM and FLM, respectively [11] and the filters were preserved at -80°C.

DNA-SIP experiments

^{13}C labeled diatom-derived detritus

Diatom species *Thalassiosira weissflogii* (strain CCMA-102) was selected for producing ^{13}C-labeled POM experiment. *T. weissflogii* was cultured according to Liu et al. [19] (see details in Additonal file 2: Supplementary method).

High-pressure incubations

The ECS surface-water microorganisms were incubated with diatom-derived POM at in-situ hydrostatic pressure (and temperature) of 0.1 (25°C), 20 (4°C) and 40 (4°C) MPa for 48–88 h in the dark. The incubation media consisted of 500 ml surface seawater, 0.15 g sterile ^{13}C-labeled particulate organic matter or ^{12}C-POM (control), and 167 ml (25% of the total volume) Fluorinert™ (3M™ Corp., Minneapolis, MN) [47]. Oxygenated-saturated Fluorinert was added to serve as a source of oxygen [47]. Two controls were prepared in a similar way: 500 mL surface seawater and 167 mL fluorinert (unamended control); 500 mL surface seawater, 0.15 g ^{12}C-control POM, 167 mL fluorinert and 300 μL 80 g/L $HgCl_2$ (killed control) [48]. Triplicate incubations were done for all treatments. Bacterial growth plateaued after 48 or 88 h.

DNA/ RNA extraction and SIP ultracentrifugation

After incubation, triplicate 350 mL of the incubation solution from ^{13}C-labeled or ^{12}C-control treatments were filtered as described above, and the filters were stored at -80°C for the molecular microbiological analysis.

The filters were first cut into pieces and then transferred to 2 mL sterilized centrifuge tubes. The DNA and RNA were extracted with RNeasy PowSoil DNA Elution Kit (QIAGEN) and RNeasy PowerSoil Total RNA Kit (QIAGEN) according to the manufacturer's protocols, respectively. The obtained total DNA and RNA pellets were dissolved in 100 μL DNase-free ddH_2O and sterile ddH_2O_{DEPC}, respectively. The concentrations of the total DNA and RNA were measured by NANODROP 2000 (Thermo Scientific, Wilmington, DE, USA), and preserved at -80°C until further analysis.

The DNA-SIP gradient fractionation was conducted by following the method as previously described [19, 49] (see details in Additonal file 2: Supplementary method).

Quantitative PCR

The copy number of bacterial 16S rRNA gene in the 3th -14th fractionated DNA of the PAM and FLM assemblages were amplified with primers Bac338F (5´-ACTCCTACGGGAGGCAGCAG-3´) and 518R (5´-ATTACCGCGGCTGCTGG-3´) [50]. The triplicate 20 μL mixture included 10 μL GoTaq® qPCR Master Mix (Promega Corporation, the USA), 2 μL of each primer (2 μM), 4 μL DNA template, and 2 μL qPCR H_2O. The detailed construction procedures of qPCR standard curve are described in Additonal file 2: Supplementary Method. The qPCR amplification performed on 7500 Real-Time PCR System (Thermo Fisher Scientific Inc., USA) with the program: initial denaturation (95°C) for 10 min; 40 cycles of denaturation at 95°C for 15 s, annealing at 60°C for 1 min, and extension at 72°C for 1 min. The amplification efficiency ranged from 95–103% and the R^2 ranged from 0.996 to 1.0. The bacterial copy number was obtained by the average of three parallel samples.

16S rRNA gene sequencing and data analysis

The total and the fractionated DNA of the PAM and FLM fractions were amplified using the barcoded primers 515F (5´-GTGYCAGCMGCCGCGGTAA-3´) and 806R (5´-GGACTACNVGGGTWT CTA AT-3´) [51], targeting the V4 region of 16S rRNA gene. The triplicate 25 μL PCR reactions contained 10 μL Premix Taq™ (Takara, China), 0.5 μL of each primer (10 μM), 10 ng of DNA, and 13 μL DNase-free ddH_2O. The PCR were conducted using the following program : 94°C for 3 min; 35 cycles of 94°C for 45 s, 50°C for 60 s, and 72°C for 90 s; 72°C for 10 min. After purification and quantification, the DNA samples was sequenced with an Illumina MiSeq platform (Illumina, San Diego, CA, United States) at the Majorbio Bio-Pharm Technology Co. Ltd. (Shanghai, China).

The raw data of 16S rRNA gene sequencing were quality-filtered by Trimmomatic (http://www.usadellab.org/cms/index.php?page = trimmomatic) [52] and assembled by FLASH (http://www.cbcb.umd.edu/software/flash) [53] according to the criteria described by Liu et al. [54]. The chimeric sequences were detected by UCHIME (http://drive5.com/uchime) [55]. The optimizing reads were clustered to operational taxonomic unit (OTU) with a cutoff value of 97% similarity using UPARSE (http://drive5.com/uparse/) [56]. The representative sequences of OTUs were classified by Ribosomal Database Project (RDP; http://rdp.cme.msu.edu/) [57] against the Silva 16S rRNA database (SSU138; http://www.arb-silva.de/) [58] using 70% of the confidence threshold.

Alpha-diversity indices (e.g., Shannon, Simpson, Ace, Chao, and Coverage) were calculated using mothur (http://www.mothur.org/) [59]. The heatmap was conducted by TBtools software (https://github.com/CJ-Chen/TBtools/releases) [60]. The Venn diagram, NMDS analysis, and the analysis of similarity (ANOSIM) were performed as previously described [19].

Ecological Network Analysis

The ecological networks were constructed based on Molecular Ecological Network Analyses Pipeline (MENAP, http://ieg4.rccc.ou.edu/mena/). Only taxa detected in more than six samples were used for

network analysis. Pearson correlation coefficients (r) between any two OTUs were estimated to generate the association matrix. The Random Matrix Theory (RMT) approach was used to determine the threshold of correlation coefficient to construct the network of non-random associations [25, 26]. Network properties were calculated using MENAP as previously described [26]. Module separation and modularity calculation were conducted by greedy modularity optimization [61], and the within-module connectivity (Zi) and among-module connectivity (Pi) [62] values for all nodes were calculated. The networks were visualized in Cytoscape (https://cytoscape.org/) [63]. Pie charts were performed by R program according to Shi et al. [64].

The nodes in the networks were divided into four topological roles based on Zi and Pi values: network hubs (highly connected nodes within entire network, $Zi \geq 2.5$, $Pi \geq 0.62$), module hubs (highly connected nodes within modules, $Zi \geq 2.5$, $Pi<0.62$), connectors (nodes that connect modules, $Zi<2.5$, $Pi \geq 0.62$), and peripherals (nodes connected in modules with few outside connections, $Zi < 2.5$, $Pi<0.62$) [24–26, 65].

Microbial community assembly processes

The relative importance of stochastic processes in microbial community assembly was quantified using the normalized stochasticity ratio (NST) [21]. The NST in this study was calculated based on Ružička dissimilarity and null model algorithm 'PF' (keep occurrence frequency proportional to observed values and richness the same as observed). The computation was performed using IEG statistical analysis pipeline (http://ieg3.rccc.ou.edu:8080) built on the Galaxy platform. NST can evaluate the community assembly as more deterministic (< 50%) or more stochastic (> 50%), with higher values indicating higher stochasticity.

Metatranscriptome Sequencing and Data Analysis

The removal of ribosomal RNAs (rRNAs) from the total RNA and construction of RNA-based library were performed by using the Ribo-zero rRNA Removal Kit (EpiCentre, WI, USA) and the TruSeq™ RNA Sample Prep Kit (Illumina, Inc., USA), respectively. Then the barcoded libraries were sequenced with an Illumina Hiseq 2500 sequencer (Illumina, USA) at Majorbio Bio-Pharm Technology Co., Ltd. (Shanghai, China).

The raw sequences were trimmed to obtain high quality pair-end reads, by applying Seqprep (https://github.com/jstjohn/SeqPrep) and Sickle (https://github.com/najoshi/sickle). Open reading frames (ORFs) were predicted with TransGeneScan (http://sourceforge.net/projects/transgenescan/). The non-redundant gene catalog was generated by using the CD-HIT (http://www.bioinformatics.org/cd-hit/) based on the sequences with > 95% sequence identity and > 90% coverage. Reads were mapped to the representative genes with 95% identity and the FPKM (fragments per kilobase of transcript per million reads mapped) were assessed with RSEM (http://deweylab.biostat.wisc.edu/rsem/). Taxonomic annotations were performed by aligning non-redundant gene catalogs against NCBI non-redundant database with e-value of $1e^{-5}$, by applying BASTP (v2.2.28+; http://blast.ncbi.nlm.nih.gov/Blast.cgi). For functional annotation, KEGG annotation was conducted by aligning non-redundant gene catalogs against

KEGG (Kyoto Encyclopedia of Genes and Genomes, http://www.genome.jp/kegg/) database, also by using BLASTP.

Declarations

Acknowledgements

We would like to thank Prof. Zhongjun Jia from the Institute of Soil Science, Chinese Academy of Sciences, China for his valuable guidance in using the SIP techniques. We thank postdoctor Jiahua Wang from the Shanghai Engineering Research Center of Hadal Science and Technology, Shanghai Ocean University, China for assistance in submission of the metatranscriptome data to the NCBI databases.

Funding

This work was supported by the National Key R&D Program of China (grant No. 2018YFC0310600), and by the National Natural Science Foundation of China (91951210, 41773069).

Availability of data and materials

All raw sequence datasets of 16S rRNA genes and metatranscriptomics sequencing from this study have been deposited into the NCBI Sequence Read Achieve (SRA) database with the accession no. PRJNA597244 and PRJNA661197, respectively.

Authors' contributions

JF designed the study and wrote the manuscript. YL did the experiments, data analysis, and wrote the manuscript. LZ helped data analysis and interpretation. MZ helped conducting the experiments. ZX, RL, and YX helped manuscript revision. DN and JZ helped data analysis and manuscript revision. All authors have read and approved the final manuscript.

Competing interests

The authors declare that they have no competing interests.

Publisher's Note

Springer Nature remains neutral with regard to jurisdictional claims in published maps and institutional affiliations.

Author details

[1]Hadal Science and Technology Research Center, Shanghai Ocean University, Shanghai 201306, PR China. [2]State Key Laboratory of Geological Process and Mineral Resources, Faculty of Earth Sciences, China University of Geosciences, Wuhan, Hubei 430074, PR China. [3]Institute for Environmental Genomics,

Department of Microbiology and Plant Biology, University of Oklahoma, Norman, OK 73019, USA. [4]School of Civil Engineering and Environmental Sciences, University of Oklahoma, Norman, OK 73019, USA. [5]Earth and Environmental Sciences, Lawrence Berkeley National Laboratory, Berkeley, CA 94704, USA. [6]State Key Joint Laboratory of Environment Simulation and Pollution Control, School of Environment, Tsinghua University, Beijing 100084, PR China. [7]Laboratory for Marine Biology and Biotechnology, Qingdao National Laboratory for Marine Science and Technology, Qingdao 266237, PR China.

References

1. Cho BC, Azam F. Major role of bacteria in biogeochemical fluxes in the ocean's interior. Nature. 1988;332(6163):441–3. https://doi.org/10.1038/332441a0.
2. Azam F, Malfatti F. Microbial structuring of marine ecosystems. Nat Rev Microbiol. 2007;5(10):782–91. https://doi.org/10.1038/nrmicro1747.
3. Anderson TR, Tang KW. Carbon cycling and POC turnover in the mesopelagic zone of the ocean: Insights from a simple model. Deep Sea Res Part II. 2010;57(16):1581–92. https://doi.org/10.1016/j.dsr2.2010.02.024.
4. Fang J, Zhang L, Li J, Kato C, Tamburini C, Zhang Y, et al. The POM-DOM piezophilic microorganism continuum (PDPMC)—The role of piezophilic microorganisms in the global ocean carbon cycle. Science China Earth Sciences. 2015;58(1):106–15. https://doi.org/10.1007/s11430-014-4985-2.
5. Grossart H-P, Tang KW, Kiørboe T, Ploug H. Comparison of cell-specific activity between free-living and attached bacteria using isolates and natural assemblages. FEMS Microbiol Lett. 2007;266(2):194–200. https://doi.org/10.1111/j.1574-6968.2006.00520.x.
6. Ghiglione JF, Mevel G, Pujo-Pay M, Mousseau L, Lebaron P, Goutx M. Diel and seasonal variations in abundance, activity, and community structure of particle-attached and free-living bacteria in NW Mediterranean Sea. Microbial ecology. 2007;54(2):217–31. https://doi.org/10.1007/s00248-006-9189-7.
7. Lapoussière A, Michel C, Starr M, Gosselin M, Poulin M. Role of free-living and particle-attached bacteria in the recycling and export of organic material in the Hudson Bay system. J Mar Syst. 2011;88(3):434–45. https://doi.org/10.1016/j.jmarsys.2010.12.003.
8. Fandino LB, Riemann L, Steward GF, Long RA, Azam F. Variations in bacterial community structure during a dinoflagellate bloom analyzed by DGGE and 16S rDNA sequencing. Aquat Microb Ecol. 2001;23(2):119–30. https://doi.org/10.3354/ame023119.
9. Li J, Wei B, Wang J, Liu Y, Dasgupta S, Zhang L, et al. Variation in abundance and community structure of particle-attached and free-living bacteria in the South China Sea. Deep Sea Res Part II. 2015;122:64–73. https://doi.org/10.1016/j.dsr2.2015.07.006.
10. DeLong EF, Franks DG, Alldredge AL. Phylogenetic diversity of aggregate-attached vs. free-living marine bacterial assemblages. Limnol Oceanogr. 1993;38(5):924–34. https://doi.org/10.4319/lo.1993.38.5.0924.

11. Eloe EA, Shulse CN, Fadrosh DW, Williamson SJ, Allen EE, Bartlett DH. Compositional differences in particle-associated and free-living microbial assemblages from an extreme deep-ocean environment. Environmental microbiology reports. 2011;3(4):449–58. https://doi.org/10.1111/j.1758-2229.2010.00223.x.
12. Crespo BG, Pommier T, Fernández-Gómez B, Pedrós-Alió C. Taxonomic composition of the particle-attached and free-living bacterial assemblages in the N orthwest M editerranean S ea analyzed by pyrosequencing of the 16S rRNA. Microbiologyopen. 2013;2(4):541–52. https://doi.org/10.1002/mbo3.92.
13. Salazar G, Cornejo-Castillo FM, Borrull E, Díez-Vives C, Lara E, Vaqué D, et al. Particle-association lifestyle is a phylogenetically conserved trait in bathypelagic prokaryotes. Molecular ecology. 2015;24(22):5692–706. https://doi.org/10.1111/mec.13419.
14. Deming JW. Bacterial growth in deep-sea sediment trap and boxcore samples. Marine ecology progress series Oldendorf. 1985;25(3):305–12. https://doi.org/10.3354/meps025305.
15. Turkey C. The effect of pressure on leucine and thymidine incorporation by free-living bacteria and by bacteria attached to sinking oceanic particles. Deep Sea Res Part I. 1993;40(11–12):2193–206. https://doi.org/10.1016/0967-0637(93)90098-N.
16. Nagata T, Tamburini C, Arístegui J, Baltar F, Bochdansky AB, Fonda-Umani S, et al. Emerging concepts on microbial processes in the bathypelagic ocean–ecology, biogeochemistry, and genomics. Deep Sea Res Part II. 2010;57(16):1519–36. https://doi.org/10.1016/j.dsr2.2010.02.019.
17. Marietou A, Bartlett DH. Effects of high hydrostatic pressure on coastal bacterial community abundance and diversity. Appl Environ Microbiol. 2014;80(19):5992–6003. https://doi.org/10.1128/AEM.02109-14.
18. Tamburini C, Garcin J, Bianchi A. Role of deep-sea bacteria in organic matter mineralization and adaptation to hydrostatic pressure conditions in the NW Mediterranean Sea. Aquat Microb Ecol. 2003;32(3):209–18. https://doi.org/10.3354/ame032209.
19. Liu Y, Fang J, Jia Z, Chen S, Zhang L, Gao W. DNA stable-isotope probing reveals potential key players for microbial decomposition and degradation of diatom-derived marine particulate matter. MicrobiologyOpen. 2020;9(5):e1013. https://doi.org/10.1002/mbo3.1013.
20. Orsi WD, Smith JM, Liu S, Liu Z, Sakamoto CM, Wilken S, et al. Diverse, uncultivated bacteria and archaea underlying the cycling of dissolved protein in the ocean. ISME J. 2016;10(9):2158–73. https://doi.org/10.1038/ismej.2016.20.
21. Ning D, Deng Y, Tiedje JM, Zhou J. A general framework for quantitatively assessing ecological stochasticity. Proceedings of the National Academy of Sciences 2019;116(34):16892-8. https://doi.org/10.1073/pnas.1904623116.
22. Zhou J, Ning D. Stochastic community assembly: does it matter in microbial ecology? Microbiol Mol Biol Rev 2017;81(4). https://doi.org/10.1128/MMBR.00002-17.
23. Faust K, Raes J. Microbial interactions: from networks to models. Nat Rev Microbiol. 2012;10(8):538–50. https://doi.org/10.1038/nrmicro2832.

24. Tu Q, Yan Q, Deng Y, Michaletz ST, Buzzard V, Weiser MD, et al. Biogeographic patterns of microbial co-occurrence ecological networks in six American forests. Soil Biol Biochem. 2020;148:107897. https://doi.org/10.1016/j.soilbio.2020.107897.
25. Zhou J, Deng Y, Luo F, He Z, Tu Q, Zhi X. Functional molecular ecological networks. MBio 2010;1(4). https://doi.org/10.1128/mBio.00169-10.
26. Deng Y, Jiang Y-H, Yang Y, He Z, Luo F, Zhou J. Molecular ecological network analyses. BMC Bioinform. 2012;13(1):1–20. https://doi.org/10.1186/1471-2105-13-113.
27. Lauro FM, McDougald D, Thomas T, Williams TJ, Egan S, Rice S, et al. The genomic basis of trophic strategy in marine bacteria. Proceedings of the National Academy of Sciences 2009;106(37):15527-33. https://doi.org/10.1073/pnas.0903507106.
28. Yooseph S, Nealson KH, Rusch DB, McCrow JP, Dupont CL, Kim M, et al. Genomic and functional adaptation in surface ocean planktonic prokaryotes. Nature. 2010;468(7320):60–6. https://doi.org/10.1038/nature09530.
29. Yang C, Wang Q, Simon PN, Liu J, Liu L, Dai X, et al. Distinct network interactions in particle-associated and free-living bacterial communities during a Microcystis aeruginosa bloom in a plateau lake. Frontiers in microbiology. 2017;8:1202. https://doi.org/10.3389/fmicb.2017.01202.
30. Ma B, Wang H, Dsouza M, Lou J, He Y, Dai Z, et al. Geographic patterns of co-occurrence network topological features for soil microbiota at continental scale in eastern China. ISME J. 2016;10(8):1891–901. https://doi.org/10.1038/ismej.2015.261.
31. Wu L, Yang Y, Chen S, Zhao M, Zhu Z, Yang S, et al. Long-term successional dynamics of microbial association networks in anaerobic digestion processes. Water Res. 2016;104:1–10. https://doi.org/10.1016/j.watres.2016.07.072.
32. Luo F, Zhong J, Yang Y, Scheuermann RH, Zhou J. Application of random matrix theory to biological networks. Phys Lett A. 2006;357(6):420–3. https://doi.org/10.1016/j.physleta.2006.04.076.
33. Chaffron S, Rehrauer H, Pernthaler J, Von Mering C. A global network of coexisting microbes from environmental and whole-genome sequence data. Genome research 2010;20(7):947–59. https://doi.org/10.1101/gr.104521.109.
34. Krause AE, Frank KA, Mason DM, Ulanowicz RE, Taylor WW. Compartments revealed in food-web structure. Nature. 2003;426(6964):282–5. https://doi.org/10.1038/nature02115.
35. Azam F, Long RA. Sea snow microcosms. Nature. 2001;414(6863):495–8. https://doi.org/10.1038/35107174.
36. Ganesh S, Parris DJ, DeLong EF, Stewart FJ. Metagenomic analysis of size-fractionated picoplankton in a marine oxygen minimum zone. ISME J. 2014;8(1):187–211. https://doi.org/10.1038/ismej.2013.144.
37. Dang H, Lovell CR. Microbial surface colonization and biofilm development in marine environments. Microbiol Mol Biol Rev. 2016;80(1):91–138. https://doi.org/10.1128/MMBR.00037-15.
38. Pegan SD, Rukseree K, Capodagli GC, Baker EA, Krasnykh O, Franzblau SG, et al. Active site loop dynamics of a class IIa fructose 1, 6-bisphosphate aldolase from Mycobacterium tuberculosis.

Biochemistry. 2013;52(5):912–25. https://doi.org/10.1021/bi300928u.

39. Maegawa Y, Morita H, Yao M, Watanabe N, Tanaka I. Crystallization and preliminary X-ray diffraction study of the catalytic subunit of archaeal H+-transporting ATP synthase from Pyrococcus horikoshii OT3. Acta Crystallogr Sect D: Biol Crystallogr. 2004;60(8):1484–6. https://doi.org/10.1107/S0907444904014222.
40. Bauer M, Kube M, Teeling H, Richter M, Lombardot T, Allers E, et al. Whole genome analysis of the marine Bacteroidetes 'Gramella forsetii'reveals adaptations to degradation of polymeric organic matter. Environ Microbiol. 2006;8(12):2201–13. https://doi.org/10.1111/j.1462-2920.2006.01152.x.
41. Lee C, Wakeham S, Arnosti C. Particulate organic matter in the sea: the composition conundrum. AMBIO: A Journal of the Human Environment. 2004;33(8):565–75. https://doi.org/10.1579/0044-7447-33.8.565.
42. Grossart HP, Czub G, Simon M. Algae–bacteria interactions and their effects on aggregation and organic matter flux in the sea. Environ Microbiol. 2006;8(6):1074–84. https://doi.org/10.1111/j.1462-2920.2006.00999.x.
43. Grossart HP. Ecological consequences of bacterioplankton lifestyles: changes in concepts are needed. Environmental Microbiology Reports. 2010;2(6):706–14. https://doi.org/10.1111/j.1758-2229.2010.00179.x.
44. Székely AJ, Berga M, Langenheder S. Mechanisms determining the fate of dispersed bacterial communities in new environments. ISME J. 2013;7(1):61–71. https://doi.org/10.1038/ismej.2012.80.
45. Liu J, Zheng Y, Lin H, Wang X, Li M, Liu Y, et al. Proliferation of hydrocarbon-degrading microbes at the bottom of the Mariana Trench. Microbiome. 2019;7(1):1–13. https://doi.org/10.1186/s40168-019-0652-3.
46. Shao Z, Wang W. Enzymes and genes involved in aerobic alkane degradation. Frontiers in microbiology. 2013;4:116. https://doi.org/10.3389/fmicb.2013.00116.
47. Fang J, Uhle M, Billmark K, Bartlett DH, Kato C. Fractionation of carbon isotopes in biosynthesis of fatty acids by a piezophilic bacterium Moritella japonica strain DSK1. Geochimica et cosmochimica acta 2006;70(7):1753–60. https://doi.org/10.1016/j.gca.2005.12.011.
48. Liu S, Wawrik B, Liu Z. Different bacterial communities involved in peptide decomposition between normoxic and hypoxic coastal waters. Frontiers in microbiology. 2017;8:353. https://doi.org/10.3389/fmicb.2017.00353.
49. Xia W, Zhang C, Zeng X, Feng Y, Weng J, Lin X, et al. Autotrophic growth of nitrifying community in an agricultural soil. ISME J. 2011;5(7):1226–36. https://doi.org/10.1038/ismej.2011.5.
50. Thijs S, Op De Beeck M, Beckers B, Truyens S, Stevens V, Van Hamme JD, et al. Comparative evaluation of four bacteria-specific primer pairs for 16S rRNA gene surveys. Frontiers in microbiology. 2017;8:494. https://doi.org/10.3389/fmicb.2017.00494.
51. Walters W, Hyde ER, Berg-Lyons D, Ackermann G, Humphrey G, Parada A, et al. Improved bacterial 16S rRNA gene (V4 and V4-5) and fungal internal transcribed spacer marker gene primers for

microbial community surveys. Msystems 2016;1(1). https://doi.org/10.1128/mSystems.00009-15.

52. Bolger AM, Lohse M, Usadel B. Trimmomatic: a flexible trimmer for Illumina sequence data. Bioinformatics. 2014;30(15):2114–20. https://doi.org/10.1093/bioinformatics/btu170.
53. Magoč T, Salzberg SL. FLASH: fast length adjustment of short reads to improve genome assemblies. Bioinformatics. 2011;27(21):2957–63. https://doi.org/10.1093/bioinformatics/btr507.
54. Liu R, Wang L, Liu Q, Wang Z, Li Z, Fang J, et al. Depth-resolved distribution of particle-attached and free-living bacterial communities in the water column of the New Britain Trench. Frontiers in microbiology. 2018;9:625. https://doi.org/10.3389/fmicb.2018.00625.
55. Edgar RC, Haas BJ, Clemente JC, Quince C, Knight R. UCHIME improves sensitivity and speed of chimera detection. Bioinformatics. 2011;27(16):2194–200. https://doi.org/10.1093/bioinformatics/btr381.
56. Edgar RC. UPARSE: highly accurate OTU sequences from microbial amplicon reads. Nature methods. 2013;10(10):996–8. https://doi.org/10.1038/nmeth.2604.
57. Cole JR, Wang Q, Fish JA, Chai B, McGarrell DM, Sun Y, et al. Ribosomal Database Project: data and tools for high throughput rRNA analysis. Nucleic acids research. 2014;42(D1):D633-D42. https://doi.org/10.1093/nar/gkt1244.
58. Quast C, Pruesse E, Yilmaz P, Gerken J, Schweer T, Yarza P, et al. The SILVA ribosomal RNA gene database project: improved data processing and web-based tools. Nucleic acids research. 2012;41(D1):D590-D6. https://doi.org/10.1093/nar/gks1219.
59. Schloss PD, Westcott SL, Ryabin T, Hall JR, Hartmann M, Hollister EB, et al. Introducing mothur: open-source, platform-independent, community-supported software for describing and comparing microbial communities. Appl Environ Microbiol. 2009;75(23):7537. https://doi.org/10.1128/AEM.01541-09.
60. Chen C, Chen H, He Y, Xia R. TBtools, a toolkit for biologists integrating various biological data handling tools with a user-friendly interface. BioRxiv 2018:289660. https://doi.org/10.1101/289660.
61. Clauset A, Newman ME, Moore C. Finding community structure in very large networks. Physical review E. 2004;70(6):066111. https://doi.org/10.1103/PhysRevE.70.066111.
62. Guimera R, Amaral LAN. Functional cartography of complex metabolic networks. nature 2005;433(7028):895–900. https://doi.org/10.1038/nature03288.
63. Shannon P, Markiel A, Ozier O, Baliga NS, Wang JT, Ramage D, et al. Cytoscape: a software environment for integrated models of biomolecular interaction networks. Genome research. 2003;13(11):2498–504. https://doi.org/10.1101/gr.1239303.
64. Shi S, Nuccio EE, Shi ZJ, He Z, Zhou J, Firestone MK. The interconnected rhizosphere: high network complexity dominates rhizosphere assemblages. Ecology letters. 2016;19(8):926–36. https://doi.org/10.1111/ele.12630.
65. Wan X, Gao Q, Zhao J, Feng J, van Nostrand JD, Yang Y, et al. Biogeographic patterns of microbial association networks in paddy soil within Eastern China. Soil Biol Biochem. 2020;142:107696. https://doi.org/10.1016/j.soilbio.2019.107696.

Figures

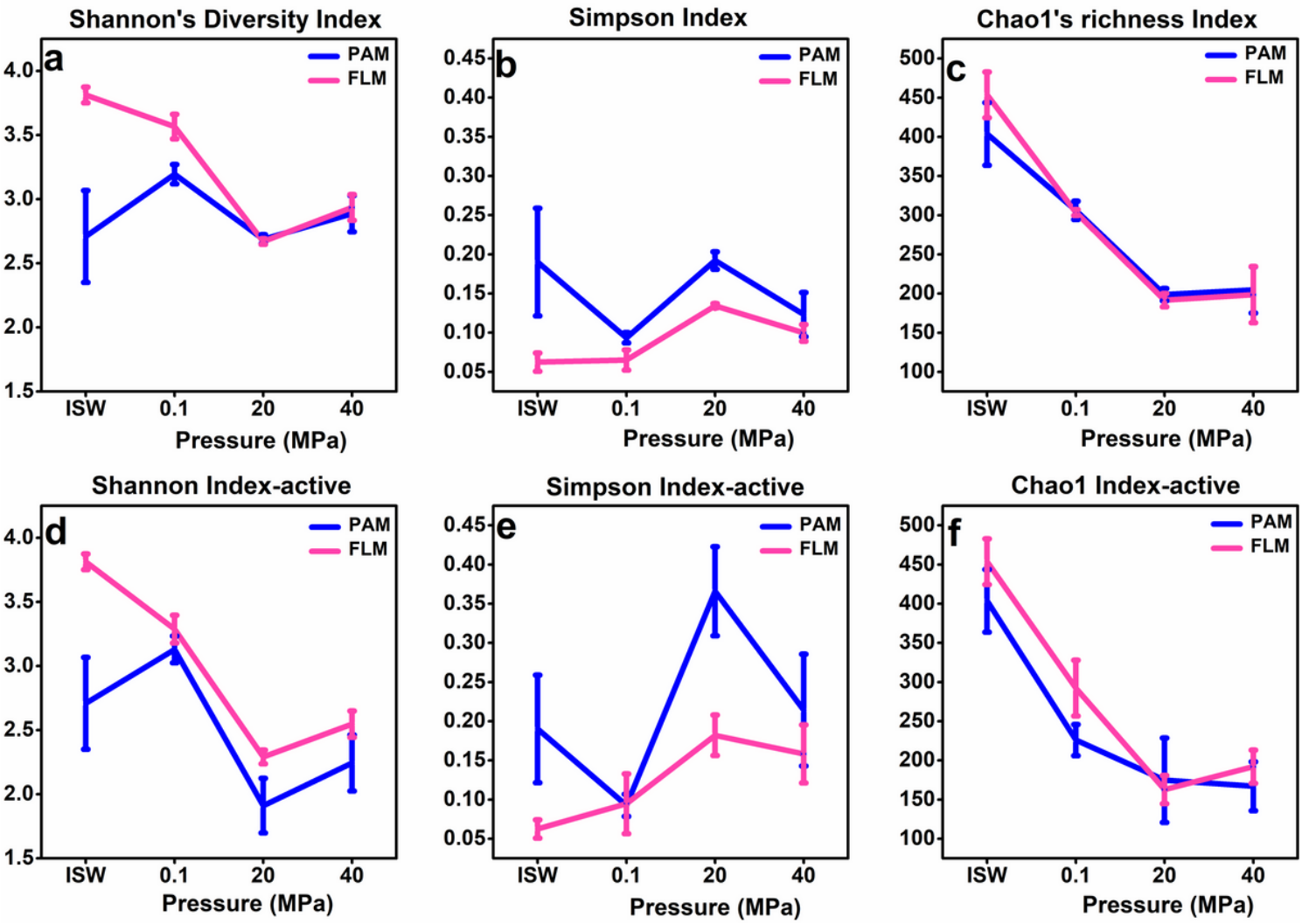

Figure 1

Alpha diversity index (Shannon index), evenness estimator (Simpson index), and richness estimator (Chao1 index) of the total and active PAM and FLM assemblages at 0.1, 20 and 40 MPa, respectively. (a) The Shannon index of the total PAM and FLM. (b) The Simpson index of the total-PAM and FLM. (c) The Chao1 index of the total PAM and FLM. (d) The Shannon index of the active PAM and FLM. (e) The Simpson index of the active PAM and FLM. (f) The Chao1 index of the active PAM and FLM. All sequences had been normalized based on the minimum number of sequences in all samples.

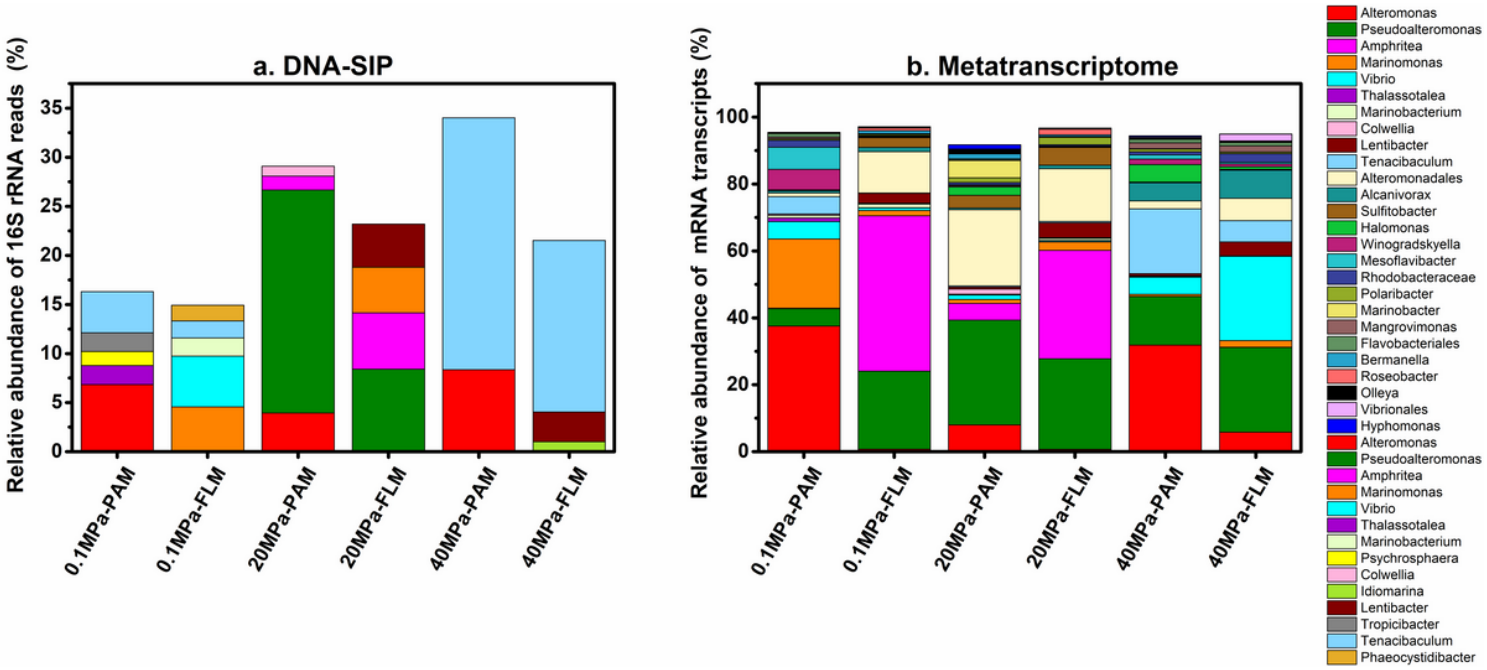

Figure 2

The most abundant active PAM and FLM taxa (>1% of the relative abundance) for POC decomposition detected by DNA-SIP and metatranscriptomic sequencing at 0.1, 20, and 40 MPa at genus level. (a) Active PAM and FLM genera identified by DNA-SIP. (b) Active PAM and FLM genera identified by metatranscriptomic sequencing.

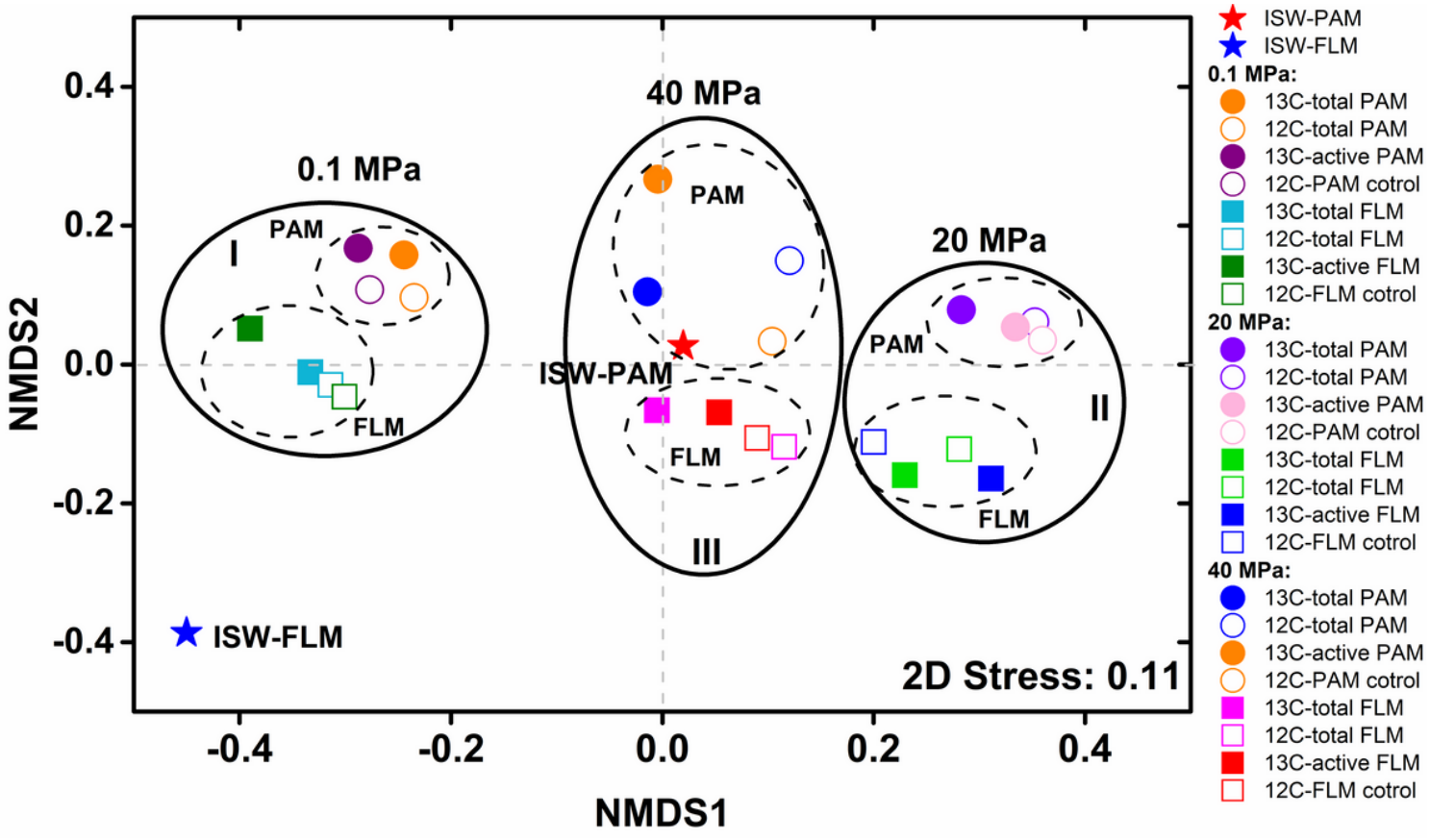

Figure 3

Nonmetric multidimensional scaling (NMDS) analysis of the total and active PAM and FLM communities incubated with 13C- or 12C-POM at 0.1, 20, and 40 MPa based on Bray-Curtis similarity matrix at the OTU level.

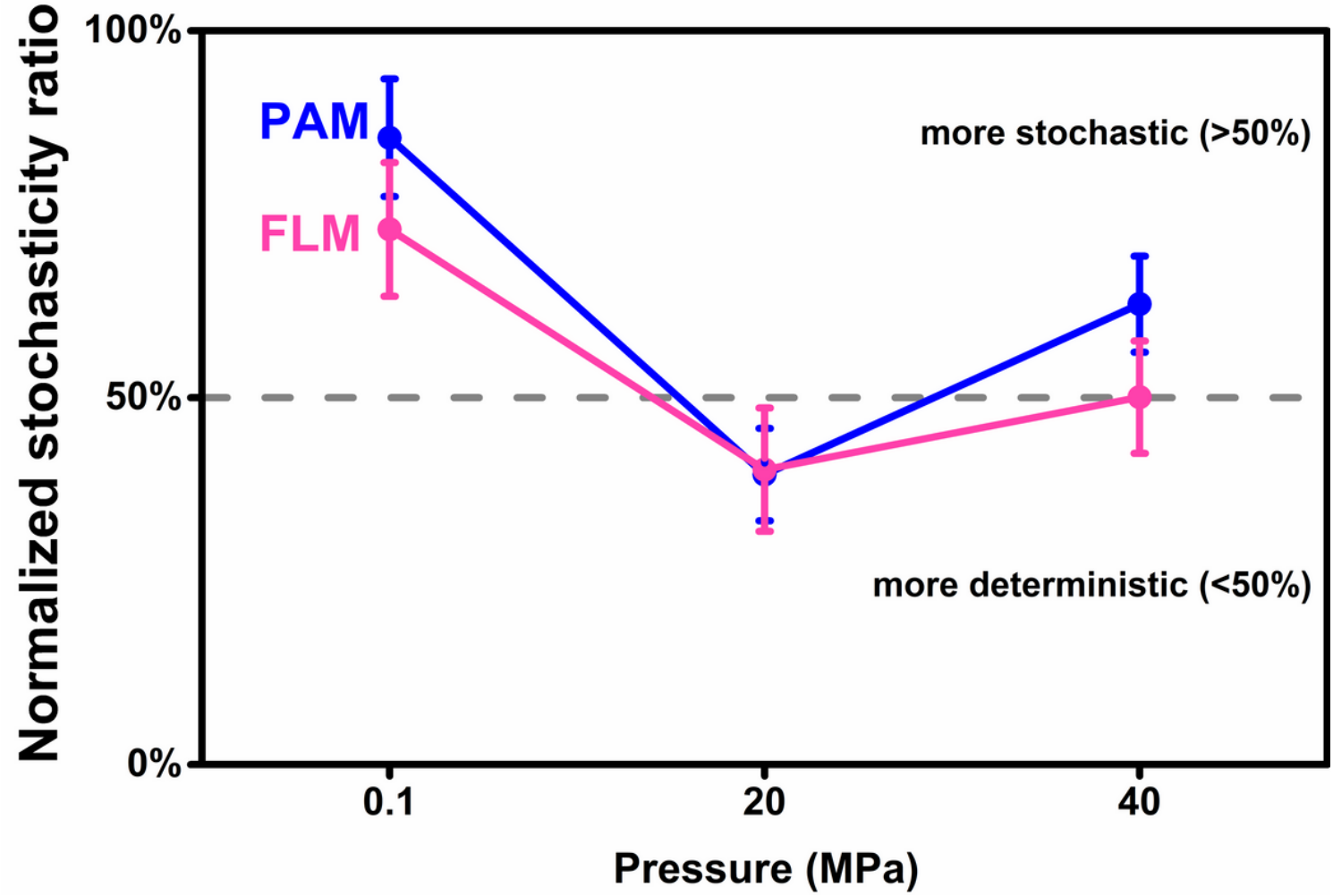

Figure 4

Variations of the normalized stochasticity ratio (NST) for the PAM and FLM microbial communities at 0.1, 20, and 40 MPa, respectively, after the addition of diatom detritus. The microbial composition tended to more stochastic (NST >50%) or more deterministic (NST <50%) based on the calculation of NST.

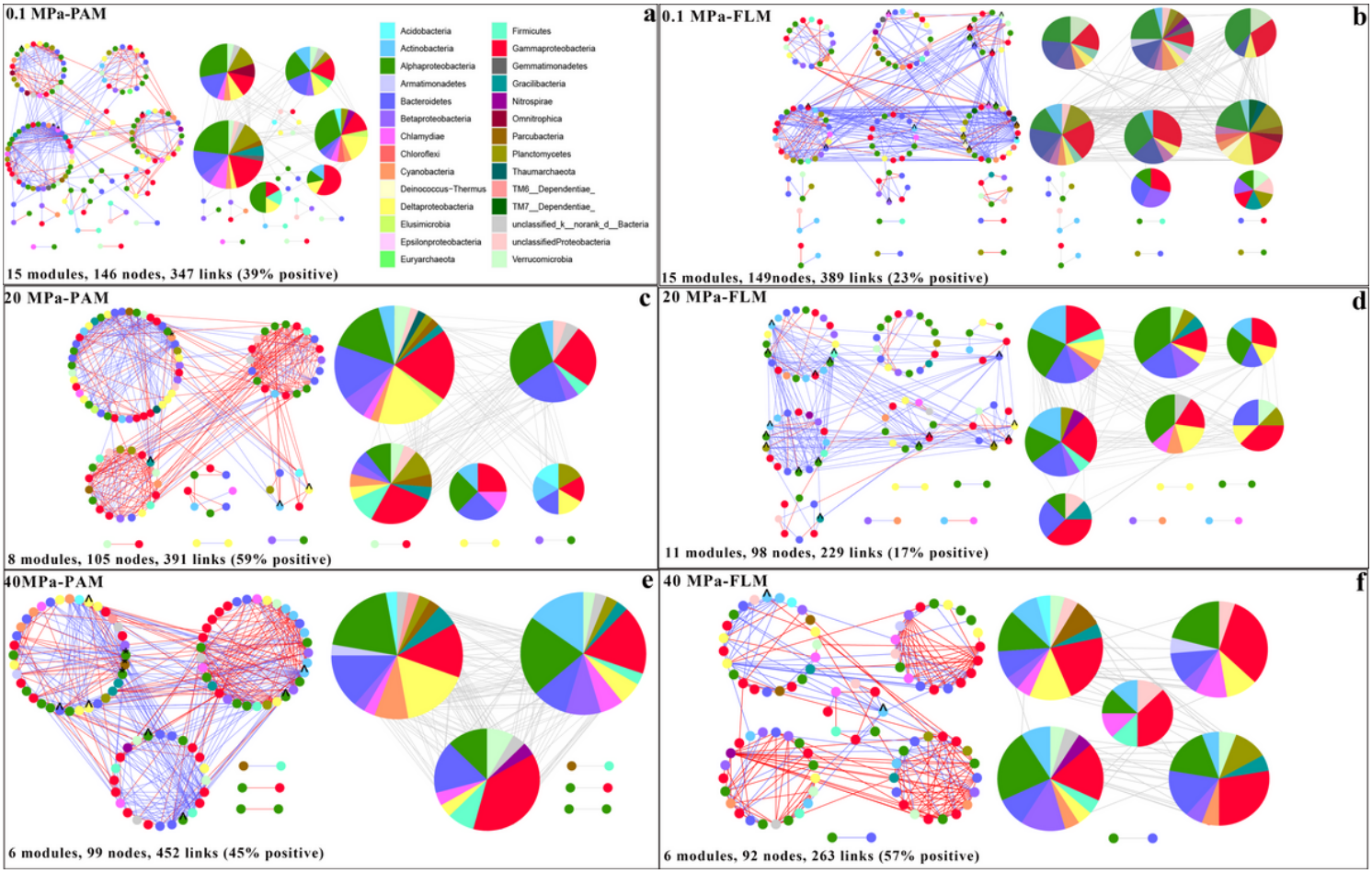

Figure 5

Network analysis of the particle-attached (PAM and free-living microbial (FLM) communities involved in POC decomposition after incubation at 0.1, 20, and 40 MPa pressures, constructed using the MENA pipeline as described in Methods. Each node represents an OTU, and color of the nodes represents different phyla or the classes of Proteobacteria. Each link represents either a positive (red line) or negative (blue line) correlation, respectively. Nodes with asterisk label (*) and label ^ represented module hubs and connectors, respectively. Pie charts show the microbial composition of different modules (> 6 nodes). (a) 0.1 MPa-PAM. (b) 0.1 MPa-FLM. (c) 20 MPa-PAM. (d) 20 MPa-FLM. (e) 40 MPa-PAM. (f) 40 MPa-FLM.

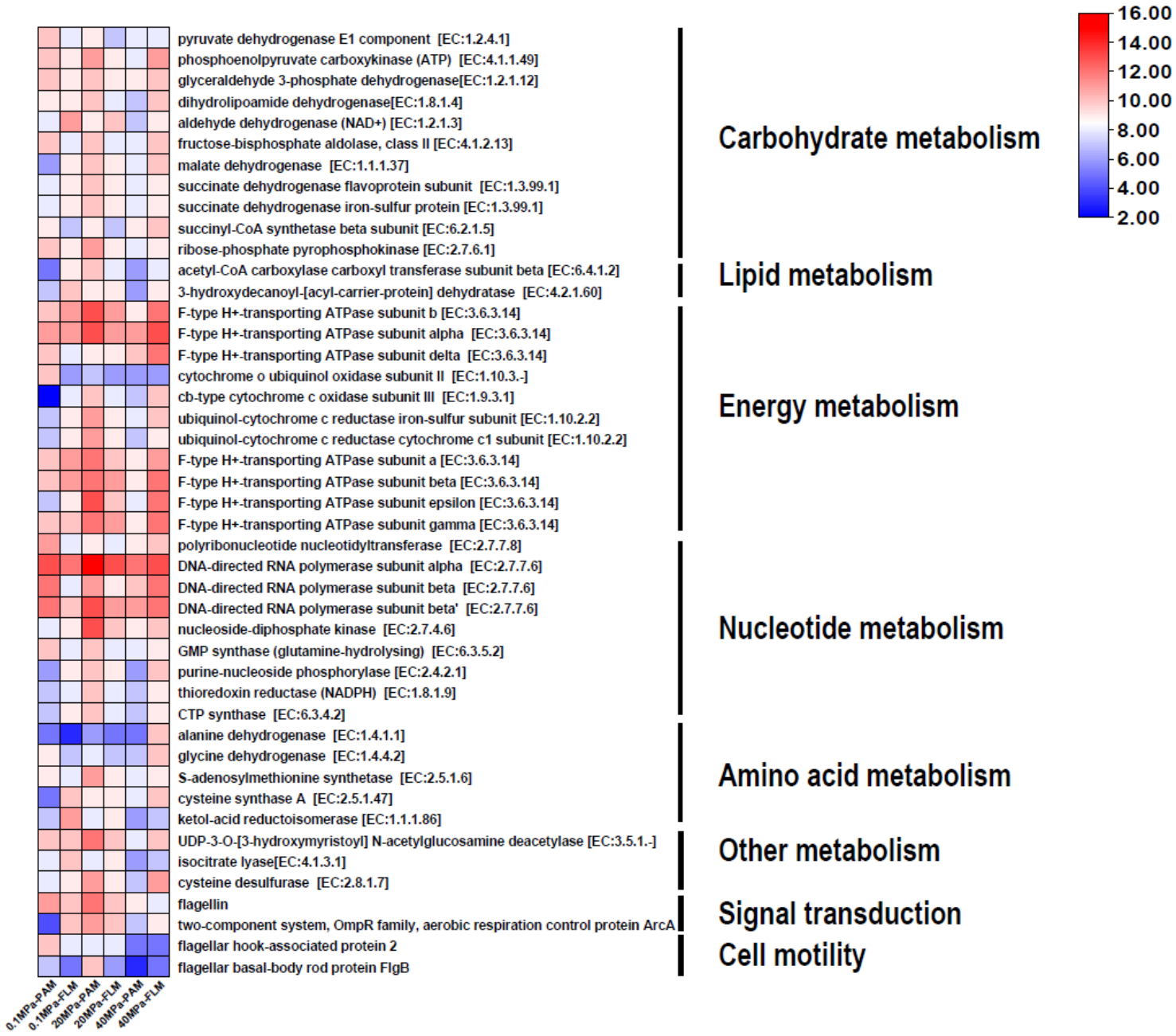

Figure 6

The 45 most abundant active functional genes and enzymes (protein) of the PAM and FLM involved in the POM decomposition and degradation annotated by KEGG orthology (KO) in the KEGG databases. Numbers shown in the legend are calculated as transformed log2 values of the normalized values.

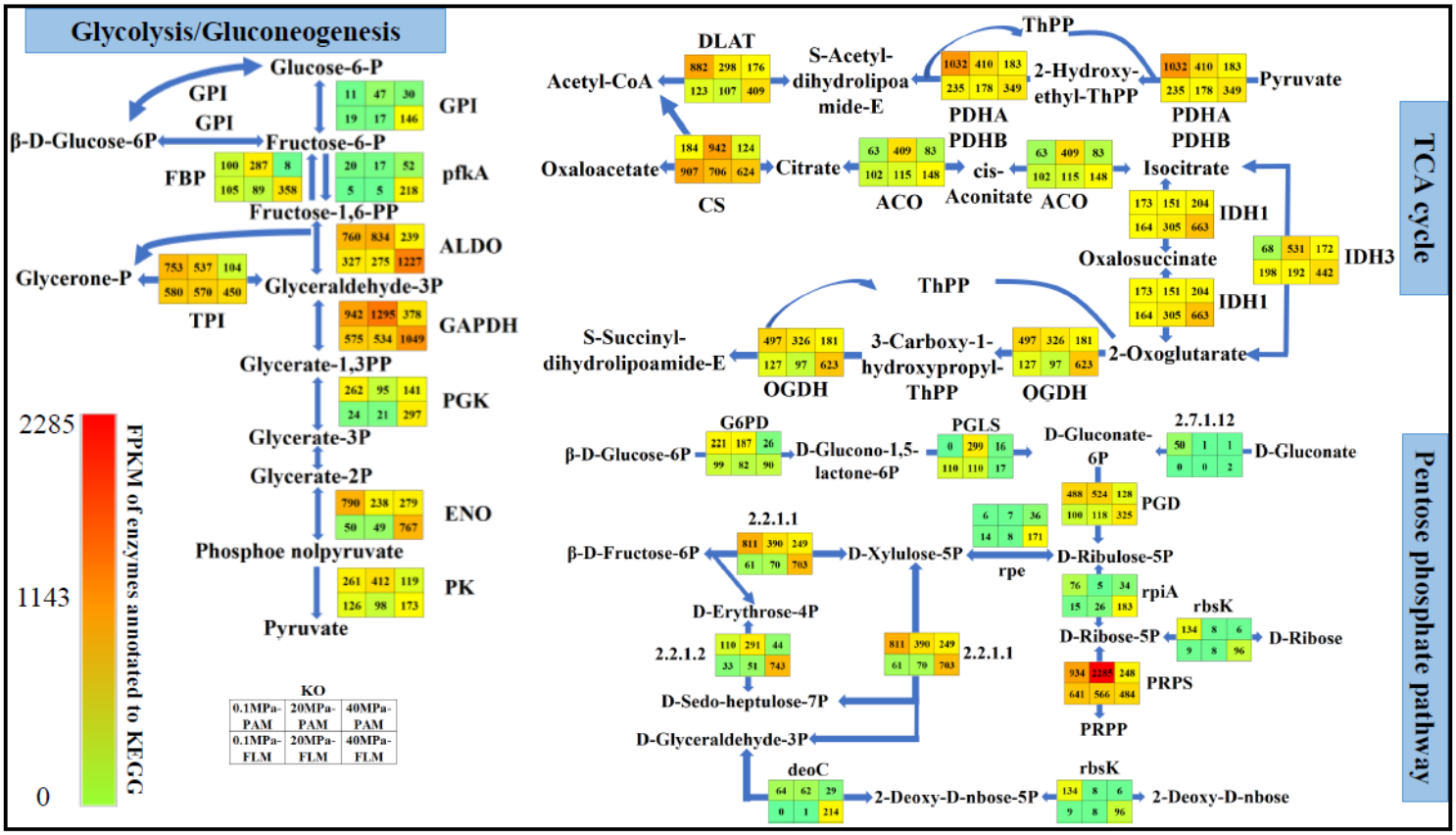

GPI	Glucose-6-phosphate isomerase (EC:5.3.1.9; K01810)
pfkA	6-phosphofructokinase 1 (EC:2.7.1.11; K00850)
FBP	Fructose-1,6-bisphosphatase I (EC:3.1.3.11; K03841)
ALDO	Fructose-bisphosphate aldolase, class I (EC:4.1.2.13; K01623)
TPI	Triosephosphate isomerase (TIM) (EC:5.3.1.1; K01803)
GAPDH	Glyceraldehyde 3-phosphate dehydrogenase (EC:1.2.1.12; K00134)
PGK	Phosphoglycerate kinase (EC:2.7.2.3; K00927)
ENO	Enolase (EC:4.2.1.11; K01689)
PK	Pyruvate kinase (EC:2.7.1.40; K00873)
DLAT	Pyruvate dehydrogenase E2 component (dihydrolipoamide acetyltransferase) (EC:2.3.1.12; K00627)
PDHA	Pyruvate dehydrogenase E1 component alpha subunit (EC:1.2.4.1; K00161)
PDHB	Pyruvate dehydrogenase E1 component beta subunit (EC:1.2.4.1; K00162)
CS	Citrate synthase (EC:2.3.3.1; K01647)
ACO	Aconitate hydratase (EC:4.2.1.3; K01681)
IDH1	Isocitrate dehydrogenase (EC:1.1.1.42; K00031)
IDH3	Isocitrate dehydrogenase (NAD+) (EC:1.1.1.41; K00030)
OGDH	2-oxoglutarate dehydrogenase E1 component (EC:1.2.4.2; K00164)
G6PD	Glucose-6-phosphate 1-dehydrogenase (EC:1.1.1.49, 1.1.1.363; K00036)
PGLS	6-phosphogluconolactonase (EC:3.1.1.31; K01057)
2.7.1.12	Gluconokinase (K00851)
PGD	6-phosphogluconate dehydrogenase (EC:1.1.1.44, 1.1.1.343; K00033)
rpe	ribulose-phosphate 3-epimerase (EC:5.1.3.1; K01783)
2.2.1.1	Transketolase (K00615)
2.2.1.2	Transaldolase (K00616)
deoC	deoxyribose-phosphate aldolase (EC:4.1.2.4; K01619)
rbsK	ribokinase (EC:2.7.1.15; K00852)
rpiA	ribose 5-phosphate isomerase A (EC:5.3.1.6; K01807)
PRPS	ribose-phosphate pyrophosphokinase (EC:2.7.6.1; K00948)

Figure 7

The expression abundance of KO genes related to carbon metabolic pathways for PAM and FLM under the three different pressures (0.1, 20, and 40 MPa). Different Colors represent the FPKM values of KO mapping to the KEGG database at 0.1, 20, and 40 MPa for PAM (upper panel) and FLM (lower panel).

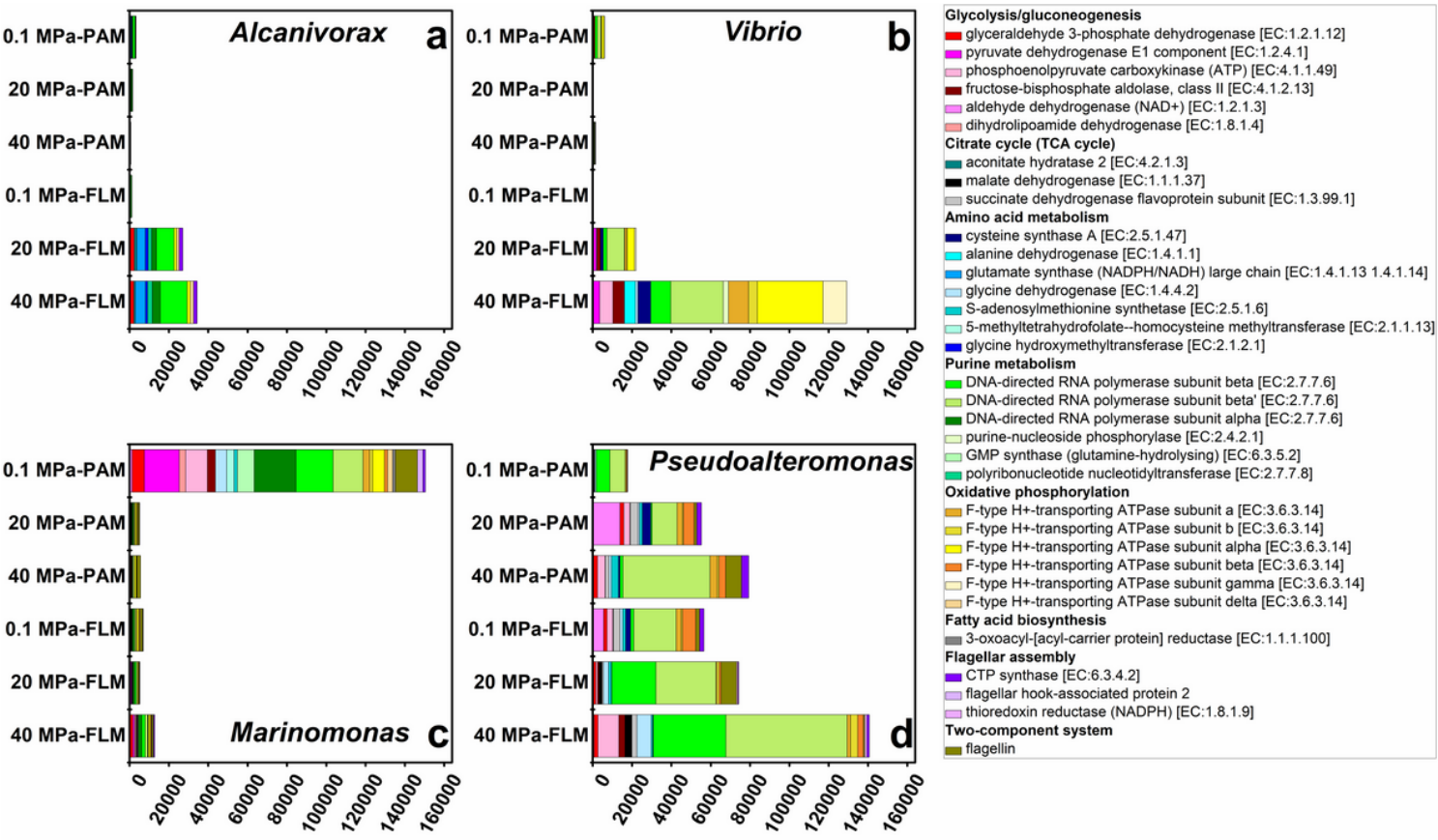

Figure 8

The active metabolic processes in POM decomposition mediated by four active taxa Alcanivorax (a), Vibrio (b), Marinomonas (c), Pseudoalteromonas (d) at 0.1, 20, and 40 MPa.

Supplementary Files

This is a list of supplementary files associated with this preprint. Click to download.

- 3Additionalfile1Microbiome6.10.docx
- 3Additionalfile2Microbiome6.10.docx